Effects of Disturbance on Seasonal CO_2 Dynamics in Two Boreal Forest Sites Underlain by Permafrost

Dragos A. Vas[1], Jaimie R. West[2], David Brodylo[1], Amanda J. Barker[1], W. Brad Baxter[1], and Robyn A. Barbato[2]

[1] U.S. Army Engineer Research and Development Center-Cold Regions Research and Engineering Laboratory, Ft. Wainwright, Alaska 99703, United States.
[2] U.S. Army Engineer Research and Development Center-Cold Regions Research and Engineering Laboratory, Hanover, New Hampshire 03755, United State.

Correspondence to Dragos Vas (Dragos.A.Vas@usace.army.mil) ORCID: 0009-0005-2319-5079.

Abstract. Permafrost regions in subarctic and arctic areas harbor substantial carbon reserves, which are becoming increasingly vulnerable to microbial decomposition as soils warm. As the seasonally thawed active layer deepens and anthropogenic disturbances escalate, accurately predicting carbon fluxes from disturbed environments underlain by permafrost requires a comprehensive understanding of soil respiration dynamics. This study investigated the impact of surface disturbance on seasonal soil biological properties in a boreal forest ecosystem near Fairbanks, Alaska. Further, we sought to identify the key environmental and geochemical factors influencing soil biology in the undisturbed and disturbed soils. Our results revealed a substantial rise in soil respiration at the disturbed boreal forest site, which exhibited a 14.4% overall increase in CO_2 efflux compared to the undisturbed site. This effect was most pronounced during the summer, when the increase in CO_2 efflux peaked at 20%. This heightened respiratory activity was directly linked to significantly warmer soil conditions, with the mean annual soil temperature at the disturbed site measuring 0.60 ± 0.16 °C, in stark contrast to the sub-zero temperatures of -0.37 ± 0.08 °C at the undisturbed site. Furthermore, the disturbed site had 30% higher bacterial community richness, 1% higher total mean C and 0.03% higher total mean N concentration levels, and 11.9% higher pH values in the subsoil layer, as well as a 147% deeper maximum active thaw depth, suggesting potential controls underlying the variation in CO_2 efflux. Our research underscores the essential importance of considering the rise in carbon emissions from anthropogenically disturbed soils underlain by permafrost, which are frequently neglected in assessments of the carbon cycle. This study contributes to a deeper understanding of the complex interactions governing soil respiration in disturbed permafrost environments, ultimately informing more accurate predictions of carbon fluxes in these ecosystems.

1. Introduction

Soil respiration, the process by which carbon dioxide (CO_2) is released from the soil surface to the atmosphere, is a critical component of the global carbon cycle. This process encompasses the

microbial breakdown of organic material as well as the respiration of plant roots. Understanding soil respiration dynamics is particularly crucial in boreal forests, as they comprise approximately 30% of global forested area and play a vital role in global carbon sequestration (Bonan, 2008; Pan *et al*., 2011; Chi *et al*., 2021). Recent studies indicate that increasing temperatures could lead to boreal forests transitioning from functioning as carbon sinks to becoming carbon sources (Bond-Lamberty *et al*., 2018; Marty *et al*., 2019, Harel *et al*., 2023). In boreal forests, soil respiration is estimated to contribute up to 68% of the total ecosystem respiration (Parker *et al*., 2020; Watts *et al*., 2021) and is significantly impacted by changes in soil temperature, soil moisture, the microbial community, and vegetation type (Grace, 2004; Fekete *et al*., 2014; Rodtassana *et al*., 2021). Soil respiration in permafrost regions is also influenced by the thickening of the active layer (the seasonally thawed soil surface layer) that occurs when permafrost is degraded due to warmer temperatures (Koster et al., 2017; Turetsky *et al*., 2020; Watts *et al*., 2021).

Anthropogenic (e.g., trail development, firewood harvesting) and natural (e.g., wildfires, insects and pathogens) disturbances fundamentally alter the landscape and soil properties, which in turn governs soil respiration and the stability of massive permafrost carbon stores (Schepaschenko et al., 2025; Miner et al., 2022). The primary disturbance agents—fire, timber harvesting, and insect outbreaks—have intensified, impacting millions of hectares annually (Schepaschenko et al., 2025). Wildfires are the dominant natural disturbance in boreal forests, and their frequency and scale have grown significantly in the recent years (Zhu et al., 2022; Schepaschenko et al., 2025). An intensified heat flux can thicken the active layer (Yoshikawa et al., 2002; Koster et al., 2017 and 20187; Zhu et al., 2022) to the point where it no longer refreezes completely in the winter, leading to the formation of a talik, or a year-round unfrozen layer of soil above the permafrost, making carbon available to microorganisms year round (Yoshikawa et al., 2002; Zhu et al., 2022).

Anthropogenic disturbances in boreal forests alter carbon cycling through distinct short- and long-term phases that are primarily driven by impacts to the underlying permafrost. Initially, disturbances like forest harvesting can cause a temporary decrease in total soil CO_2 efflux by eliminating root (autotrophic) respiration (Akande et al., 2023; Schepaschenko et al., 2025). However, this short-term effect is overshadowed by the dominant, long-term consequences of physical changes to the ground's thermal regime. Activities such as land clearing for infrastructure and resource exploration remove the insulating vegetation and surface organic layers, leading to warmer soil temperatures and a deeper active layer (Forbes et al., 2002; Foster et al., 2022). This permafrost degradation exposes vast stores of previously frozen organic carbon to microbial decomposition, transforming the disturbed landscape into a persistent, long-term source of atmospheric CO_2 (Koster et al., 2018; Miner et al., 2022). As ecosystems

recover, the combination of this sustained decomposition with new root respiration can lead to total soil efflux rates that ultimately exceed those of undisturbed forests (Akande et al., 2023). Consequently, these human disturbances are a critical factor that accelerates the permafrost carbon feedback, significantly impacting the overall carbon balance of the circumpolar north (Schepaschenko et al., 2025; Miner et al., 2022).

Despite their importance, the cumulative impacts of these anthropogenic disturbances on landscape and soil properties are not well understood, often being overshadowed by the more extensively studied effects of wildfire (Foster et al., 2022). Therefore, investigating soil respiration in disturbed, permafrost-affected environments is crucial for assessing the resilience and vulnerability of boreal ecosystems. Under projected climate scenarios, the frequency and intensity of disturbances in these regions are expected to increase, potentially leading to significant changes in soil carbon fluxes (Schepaschenko et al., 2025). Further, insights gained from such studies can inform forest management practices aimed at mitigating the impacts of disturbances and preserving the carbon sequestration potential of boreal forests.

The aim of this study is to measure and compare the soil respiration rates in undisturbed and disturbed sites in a subarctic boreal forest. The disturbance was due to historical activities related to mining, such as trail development and firewood harvest. These disturbances took place in the early 1920s, coinciding with the construction of a drainage ditch and an access trail to support mining operations in the area. During the trail and draining ditch development, the groundcover vegetations and surface soils were disturbed, and the trees were harvested. Currently, there is no active drainage at the research site, and the trail is seldom used. We hypothesize that the disturbance had a lasting effect on soil activity and properties and there will be a significant difference in the measurements between the undisturbed and disturbed sites. Further, we hypothesize that this trend also occurs in winter, where measurements are severely lacking, though soils are active.

To reveal the fundamental controls driving variation in soil respiration within and between the disturbed and undisturbed boreal forest sites, we examined seasonal soil CO_2 efflux alongside various edaphic factors, including soil temperature, moisture content, soil organic matter (SOM), pH, and the composition of microbial communities. To assess this relationship, a non-linear Random Forest Model (RFM) was used in conjunction with regression analysis to analyze the time series data, which encompassed variables such as soil respiration, temperature, moisture, and air temperature. Additionally, R statistical ANOVA analysis was performed to evaluate soil characteristics, particularly pH and SOM, as well as the composition of soil microbial communities. The emissions data and estimates of carbon fluxes will be helpful to improve carbon modeling efforts. In the following sections, we detail the study site and

99 our methodological approach (Section 2), present the key findings related to soil conditions and
100 respiration (Section 3), and discuss the implications of these findings for understanding carbon cycling in
101 disturbed permafrost ecosystems (Section 4).

102 **2. Materials and Methods**

103 **2.1 Site description**

104 The study was conducted at two adjacent sites underlain by permafrost in a subarctic boreal
105 forest, of the discontinuous permafrost region, located at the U.S. Army Cold Regions Research and
106 Engineering Laboratory (CRREL) Permafrost Research Tunnel Facility in Fox, Alaska (64.9507 N -
107 147.6200 W, 248 m a.s.l.). The region experiences a continental climate, which is defined by an average
108 annual air temperature of −2.4 °C, with average temperatures in July reaching 16 °C and January
109 temperatures averaging −21.9 °C; extreme temperatures throughout the year can range from −51 °C to
110 38 °C (Jorgenson et al. 2020). The two sites were situated approximately 10 m apart (Figure 1) and
111 exhibited comparable topography and parent material. The first site consists of an undisturbed black
112 spruce forest ecosystem (SI Figure S1); the second consists of an anthropogenically disturbed area where
113 trails were established, and black spruce tree cover was removed in firewood harvests during mining
114 activities in the region in the 1920s.

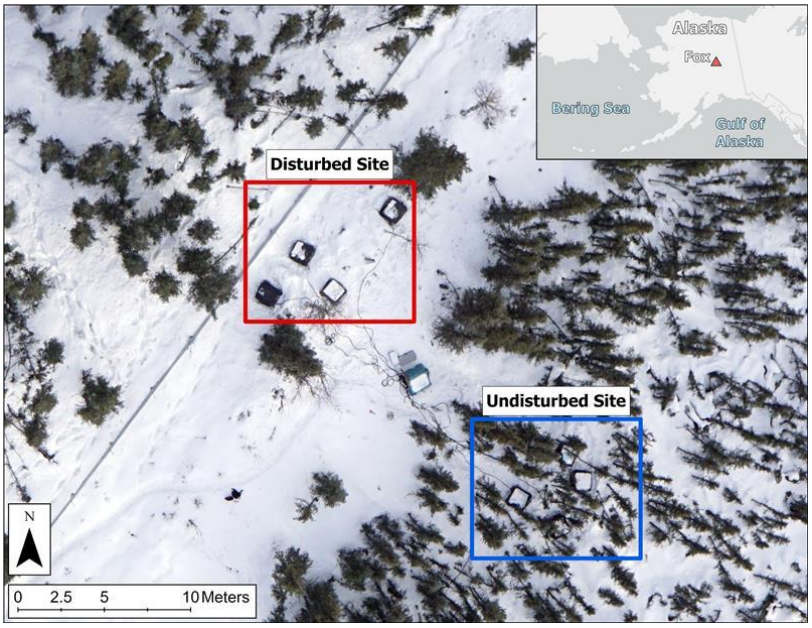

115

116 **Figure 1**. Aerial view of the study sites and experimental setup. The image displays the geographical
117 location and the layout of the sample plots at the undisturbed (blue rectangle) and disturbed (red

rectangle) study sites. The aerial image was captured on March 18, 2023. (Image credit: Dr. David Brodylo).

The vegetation at the undisturbed site consists of small black spruce (*Picea mariana*) ranging from densely distributed to tightly spaced. Understory canopy is dominated by marsh and bog Labrador tea (*Rhododendron tomentosum*; *groenlandicum*). Forest floor cover is primarily mosses (i.e., feather mosses and *Sphagnum spp.*) and small shrubs including lowbush cranberry (*Vaccinium vitis-idaea*). The disturbed site is characterized by scattered birch (*Betula neoalaskana*) and tall black spruce (*Picea mariana*) cover. The understory canopy is primarily dwarf shrubs including marsh Labrador tea and bog blueberry (*Vaccinium uliginosum*). The ground surface cover is dominated by grasses (*Poaceae*) and sedges (*Cyperaceae*). The typical undisturbed soil profile at this site consists of a fibric organic layer of variable thickness, which primarily contains undecayed and partially decayed moss and forest litter materials (O horizon), underlain by an organic-rich mineral material layer containing hemic-sapric organic fraction (A/B horizon), and thick accumulations of mineral material at the base (B/C horizon). Disturbance seemingly impacts the thickness of the surface organic layer. Soil sampling at each site targeted soil materials below the organic horizon. The sampled soil material at the two sites were classified as mineral soil material (<20% organic matter [OM]; Soil Survey Staff, 2022) with a subdivision of more organic-rich fractions (10-18% OM) comprising a "topsoil" layer (akin to an A horizon) that starts below the organic layer (O horizon), and more mineral-rich material (<5% OM) comprising a "subsoil" layer. The topsoil textures ranged from loam to silt loam, reflecting a higher proportion of sand particles in the topsoil relative to the silt loam-textured subsoil (SI Table 1).

2.2. Installation of soil and meteorological sensors

Four plots were established at an undisturbed site, and the other four were located at an adjacent disturbed site (Figure 1). At each site, sensors were distributed to measure total soil respiration (autotrophic and heterotrophic), temperature, and volumetric water content (VWC) every 30 minutes from November 4, 2022, to November 9, 2023. During the same period, air temperature and barometric pressure were recorded every 15 minutes. Because some of the sensors have robotic arms to collect measurements that would be impeded by snowfall in the winter, Costco folding tables (Columbus, Indiana) with a surface of 91.4 cm × 91.4 cm were situated above the plots, during that period, to prevent snow accumulation (Figure 2b). The folding tables were removed at the onset of the snow-free season to reduce interference with natural environmental factors such as rain and solar radiation (Figure 2c).

Soil temperature, VWC, air temperature, and barometric pressure were measured using the following Onset HOBO (Onset, Bourne, Massachusetts, USA) instrumentation: U30 USB Weather Station, S-TMB-M002 12-Bit Temperature Smart Sensor, S-SMC-M005 EC5 Soil Moisture Smart

Sensor, S-THC-M002 Temperature/Relative Humidity Smart Sensor, and S-BPB-CM50 Smart Barometric Pressure Sensor. Soil temperature and VWC were recorded in the topsoil and subsoil layers, approximately 30 cm from each soil respiration sensor, at a depth of 18.5 ± 1.19 cm in the topsoil layer and 34.5 ± 1.47 cm in the subsoil layer for the undisturbed site. At the disturbed site, the measurements were taken at 13.5 ± 2.53 cm in the topsoil layer and 35.5 ± 1.85 cm in the subsoil layer. These depths were measured from the top of the ground vegetation cover (the moss surface). At both sites, the temperature and VWC sensors of the topsoil were installed below the fibric organic layer that had a thickness of 16.5 ± 1.19 cm at the undisturbed site and 9.5 ± 0.87 cm at the disturbed site. The differences in sensor placement depth were influenced by the variations in the thickness of the organic layer between the two sites (SI Figure S2). VWC measurements were restricted to the summer and autumn seasons due to the sensor's inability to measure below freezing temperatures. Air temperature and barometric pressure were measured at 2 m above the substrate surface.

The depth of thaw in the active layer was assessed at ~ 10 cm from each of the eight chamber plots during each site visit (n = 160) from 12 May to 3 Oct 2023. To determine this depth, a graduated metal rod with a diameter of 1 cm (known as a frost probe) was inserted into the ground, at the same location, until it met resistance, establishing the distance between the ground surface vegetation and the top of the frozen soils (Shiklomanov *et al*. 2013).

For the soil respiration measurements, which encompasses the overall release of CO_2 from the soil into the atmosphere (including both autotrophic and heterotrophic processes), we installed 21.3 cm diameter thick-walled polyvinyl chloride (PVC) collars (LI-COR inc., Lincoln, Nebraska, USA) in the center of each plot. They were a height of 11.4 cm and were inserted 2-3 cm into the soil through the soil vegetation cover. The collars spacing varied from two to four meters at the undisturbed site and from three to eight meters at the disturbed site (Figure 1). We installed a 8200-104 Opaque Long-Term Chamber (LI-COR inc., Lincoln, Nebraska, USA) above each collar, which yielded a total of eight. The chambers were connected via 15 m long tubing and cable assembly to a LI-8250 multiplexer (LI-COR inc., Lincoln, Nebraska, USA) that linked to a LI-870 CO_2/H_20 gas analyzer (LI-COR inc., Lincoln, Nebraska, USA). The cable and tubing assembly was wrapped in 1.3 cm thick tubular pipe insulation foam to prevent internal clogging from freezing moisture to ensure data collection in winter.

2.3 Respiration Data Collection

The measurement process followed a closed-chamber dynamic methodology, which was automated and controlled by the LI-8250 Multiplexer. At 30-minute intervals, the multiplexer would initiate a measurement at one of the chamber locations. This involved the 8200-104 chamber

automatically rotating and lowering to seal onto the pre-installed PVC soil collar, creating a closed headspace over the soil surface. Once the chamber was sealed, the LI-8250 directed a closed loop of air from the chamber headspace to the LI-870 and LI-7810 analyzers and back. The gas analyzers measured CO_2 and H_2O concentrations, for a period of 120 seconds, at a rate of 1 Hz. As CO_2 was respired, its concentration within the closed system increased over time. The soil CO_2 flux was calculated from the rate of this concentration increase. After each measurement cycle, the chamber automatically opened, and the system proceeded to the next chamber in the sequence. A more detailed description of the soil gas flux system's operation and these winter modifications can be found in Vas et al. (2023).

Throughout the year, we performed site visits on a near-weekly basis to download data and maintain the equipment. Standard maintenance involved visually inspecting each chamber and clearing the seals of any debris. During winter months, this was supplemented by ensuring the protective tables remained free of deep snow, a necessary step to allow for sufficient air exchange to ensure the accuracy of the measurements.

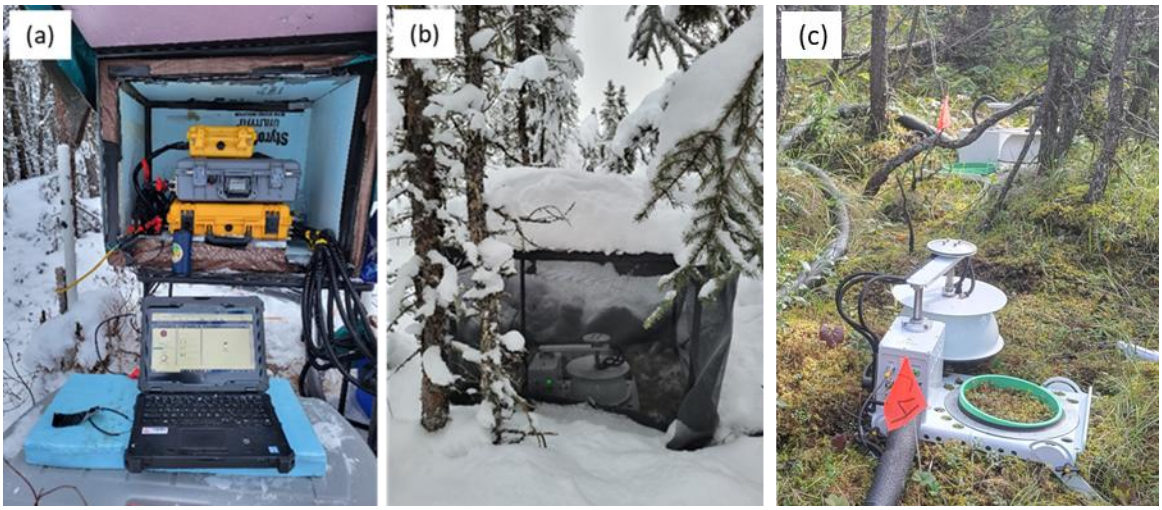

Figure 2. Custom modifications for LI-COR Soil gas flux system in cold climates. Enclosures were designed to ensure optimal operating temperatures (**a**) (photo credits: Dragos A. Vas, 17 November 2023), insulated tubing for instruments to prevent clogging, and long-term covers for chambers (**b**) (photo credits: Dragos A. Vas, 13 January 2023) to inhibit snow accumulation or drifting on the chambers. Snow free season photo of the chamber (**c**) (photo credits: Dragos A. Vas, 13 August 2023); the long-term covers were removed at the beginning of the snow free season.

2.5 Soil collection and property analysis

Soil samples were collected from both the topsoil and subsoil layers across all plots in the autumn (September 2022), winter (February 2023), and summer (June 2023) seasons to analyze potential variations in microbial community composition among seasons, disturbance regimes, and soil layers. The

samples were collected at identical depths during each season, which coincided with the depth at which the soil temperature and moisture probes were positioned; these depths varied for each plot according to the organic layer thickness. The winter samples were acquired using a gas-powered SIPRE (Snow, Ice, and Permafrost Research Establishment) corer (Jon's Machine Shop, Fairbanks, Alaska, USA). Nitrile gloves were utilized to minimize any potential contamination to the cores. Furthermore, the SIPRE corer and all associated tools were thoroughly sanitized with 70% isopropyl alcohol, DNA away, and RNase away (Thermo Fisher Scientific in Waltham, MA, USA). The cores were then subsampled into approximately 5 cm long cylinders using a sanitized hammer and chisel and were carefully placed into sterile Nasco™ Whirl-pak bags (Thermo Fisher Scientific, Waltham, MA, USA); further information on this sampling method can be found in Barbato *et al*. (2022). Summer and autumn soil samples were gathered using a sanitized trowel with 70% isopropyl alcohol, DNA away, and RNase away. The samples, approximately 5 cm thick, were placed in sterile Nasco™ Whirl-pak bags and immediately placed in a cooler with frozen ice packs, then transferred to a freezer upon arrival at the Cold Regions Research and Engineering Laboratory in Fairbanks, Alaska (CRREL-AK). All collected soil samples were kept at a temperature of -25 °C until shipped to CRREL in Hanover, New Hampshire (CRREL-NH), where they were stored at -20 °C until further processing. Deep freezing the soil samples immediately after collection and maintaining this state until processing halts microbial growth and facilitates the preservation of the microbial community structure at the moment of sampling (Baker et al., 2023; Doherty et al., 2020).

Loss on ignition (LOI) was measured as a proxy for SOM content (Storer, 1984) on all soil samples. Here, LOI is the proportion of mass loss from oven-dried soil (dried at 105 °C for 24 hours) following 2 hours at 360 °C in a muffle furnace. Soil total carbon and total nitrogen was measured via combustion using a TruSpec C and N Analyzer (LECO, St. Joseph, MI, USA) at the University of Wisconsin Soil and Forage Lab. Soil pH was measured from a 1:1 slurry of soil: $CaCl_2$ solution (0.01M) using a pH probe (Hanna Instruments, Woonsocket, RI, USA) and a SevenEasy S20 pH meter (Mettler Toledo, Columbus, OH, USA). Soil pH was converted to H+ concentration prior to taking an average or statistical analysis. LOI total carbon, total nitrogen and soil pH were statistically analyzed using ANOVA in R.

2.6 Soil microbial DNA extraction, gene sequencing, and data analysis

Soil was partially defrosted and homogenized in the sample bag prior to subsampling 250 mg into bead beating tubes. Total genomic DNA was extracted using the DNeasy PowerSoil Pro Kit (Catalog No. 47014, Qiagen, Germantown, MD, USA), using a Precellys Evolution Touch homogenizer for the bead beating step (Catalog number P002511-PEVT0-A.0, Bertin Technologies, Montigny-le-Bretonneux,

239 France). Automated DNA extraction was done with a QIAcube Connect (Catalog No. 9002864, Qiagen,
240 Germantown, MD, USA) and each extraction run included a blank. Extracted DNA was held at -20 °C.

241 Library preparation and sequencing was completed at Argonne National Laboratory (Lemont, IL,
242 USA), as follows. For bacterial analysis, the V4 region of the 16S rRNA gene was targeted for PCR
243 amplification with region-specific primers (forward primer 515F and reverse primer 806R); and for
244 fungal analysis, the ITS region was amplified using appropriate barcoded primers (Caporaso *et al*., 2011;
245 Caporaso *et al*., 2012; Apprill *et al*., 2015; Parada *et al.*, 2016; Smith *et al*., 2014; Walters *et al*., 2016).
246 Each PCR reaction contained 1 µL template DNA, 12.5 µL AccuStart II PCR ToughMix (Quantabio,
247 Beverly, MA, USA), 1 µL forward primer with Golay barcode (5 µM concentration), 1 µL reverse primer
248 (5 µM concentration), and 9.5 µL DNA-free PCR water. PCR conditions were: 94 °C (3 minutes to
249 denature the DNA); 35 cycles of 94 °C (45 s), 50 °C (60 s), and 72 °C (90 s); final extension at 72 °C (10
250 minutes). PCR product was quantified using Quant-iT PicoGreen (P7589, Invitrogen, Waltham, MA,
251 USA). Equimolar amounts of amplicons were pooled, purified using AMPure XP Beads (A63881,
252 Beckman Coulter, Brea, CA, USA), quantified (Qubit, Invitrogen), and diluted to 6.75 pM using a 10%
253 PhiX spike. Paired-end 2 x 251 sequencing was done on a MiSeq (Illumina, San Diego, CA, USA).

254 Sequencing data were processed in R (R-Core-Team, 2018), using a dada2 v1.18.0 pipeline
255 (Callahan et al., 2016), as in Baker et al. (2023), implemented using Snakemake v7.25.0 (Mölder et al.,
256 2021). Taxonomy assignment was based on the SILVA 138.1 reference database for 16S sequences (Quast
257 *et al*., 2013; Yilmaz et al., 2013) and the UNITE database (release 25.07.2023) for ITS sequences (Kõljalg
258 *et al*., 2013; Nilsson *et al*., 2019). Chloroplasts and mitochondria were excluded from the dataset. A total
259 of 2836 fungal ASVs and 10,608 bacterial ASVs were identified (excluding extraction blanks). Amplicon
260 sequences are in the National Center for Biotechnology Information Sequence Read Archive (NCBI
261 SRA), accession PRJNA1178745. Though our bacterial primers targeted both bacterial and archaeal 16S
262 rRNA, we will refer simply to bacteria, which comprise 99.8% of total reads. Of archeal reads, 80%
263 represented the phylum *Crenarchaeota*. One sample was excluded from analysis because it was
264 mislabeled (2023_Feb, Chamber 3, Organic).

265 R software (R-Core-Team, 2018), and *ggplot2* (Wickham, 2016) were used for data analysis and
266 visualization; the bioinformatic approach followed West et al. (2022). Community composition was
267 visualized using principal coordinates analysis (PCoA) of Bray-Curtis dissimilarities (Bray and Curtis,
268 1957) generated using *avgdist* from the R package *vegan* (Oksanen *et al*., 2024) using rarefaction (999
269 iterations) to a sampling depth of 16,300 for 16S and 6150 for ITS. A significant effect ($p < 0.05$) of
270 disturbance, sampling date, and interaction of these factors on community composition was tested within
271 each soil layer (topsoil and subsoil), using permutational multivariate analysis of variance

(PERMANOVA; *adonis2* from *vegan*) (Anderson, 2001). Richness was evaluated using weighted linear regression (*betta* function in *breakaway* R package) (Willis *et al*., 2017), and a significant effect of disturbance tested via ANOVA. Differential abundance (*differentialTest* in the *corncob* package) (Martin *et al*., 2021) was then used to identify significant enrichment or depletion of individual taxa due to disturbance, after excluding taxa with mean relative abundance < 0.00001.

2.7 Linear regression analysis

For statistical analysis, data on soil respiration, soil temperature, and VWC, as well as air temperature and barometric pressure from the eight chamber plots (four located at the disturbed site and four at the undisturbed site), were averaged to obtain daily means (n=333 per variable) and seasonal means (n=4 per variable). Seasons were defined according to observed efflux seasonality at the research site, a classification consistent with previous research on boreal forest efflux (Wats et al., 2021): winter (November to March, n=123), spring (April to May, n=57), summer (June to August, n=92), and autumn (September to October, n=61). Using these processed data, we performed a series of linear regression analyses to determine the existence of distinct, linear trends between CO_2 efflux and each environmental variable. This analysis was conducted separately for each site and season, and the coefficient of determination (R^2) was calculated to quantify the strength of each trend. Additionally, a one-way Analysis of Variance (ANOVA) was used to test for statistically significant differences between the disturbed and undisturbed sites. A p-value of less than 0.05 was considered significant for all tests. All statistical linear regression analyses were conducted using Microsoft Excel.

2.8 Random Forest modeling

A regression-based Random Forest (RF) non-linear model developed in R was used to identify the relative importance of the input variables to predict hourly and daily CO_2 concentrations. RF was chosen over other algorithms due to its wide and successful application in determining variable importance (Behnamian *et al*., 2017; Lei *et al*., 2024). In RF, the supervised non-linear algorithm can combine predictions from hundreds or thousands of individual decision trees via bootstrap aggregation to generate an ideal output (Schonlau and Zou, 2020). Compared with individual decision trees, this results in an increase in generalization accuracy and a reduction in overfitting. A repeated k-fold cross-validation technique was also employed. In this technique, data are randomly separated into *k* subsets with *k*-1 used to train the model and the remainder to test the model, which is then repeated a specified amount. We selected a value of 10 for k and a value of 5 for repetition. Input variables were the same for each instance except barometric pressure being dropped for daily CO_2 concentrations due to poor importance values. Thaw depth was static in the dataset that the model used from 4 October through 16 May due to the

presence of a frozen surface layer preventing thaw depth probing. Organic soil VWC and mineral soil VWC from 1 November – 31 March and 1 April – 31 May were omitted for machine learning due to the inability of the probes to function properly in subzero temperatures.

3. Results

3.1 Soil conditions

Soil temperature fluctuated by a factor of three at the disturbed site and by a factor of 1.9 at the undisturbed site over the course of the year. The undisturbed and disturbed sites exhibited contrasting thermal regimes. At the undisturbed site, the mean annual soil temperatures were below freezing, exhibiting -0.33 ± 0.1 °C for topsoil and -0.41 ± 0.07 °C for subsoil (Figure 3). In contrast, the disturbed site experienced positive mean annual soil temperatures, with 0.72 ± 0.2 °C for topsoil and 0.48 ± 0.13 °C for subsoil. Winter was the only season with warmer topsoil and subsoil temperatures at the undisturbed site. For both the undisturbed and disturbed sites, the subsoil layer was cooler than the topsoil layer in terms of mean annual temperature. Significantly warmer soil temperatures were observed at the disturbed site during the summer (4.04 ± 0.19 °C; p <0.001, ANOVA) and autumn (1.88 ± 0.23 °C; p <0.001, ANOVA) in comparison to the temperatures recorded at the undisturbed site during the same seasons. Conversely, the mean summer soil temperature at the undisturbed site was 1.15 ± 0.08°C, while the mean autumn soil temperature was 0.38 ± 0.07 °C (Figure 3). Soil temperatures in the shallower topsoil layer exhibited greater variability throughout the year compared to the temperatures in the deeper subsoil layer at both sites (Figure 3).

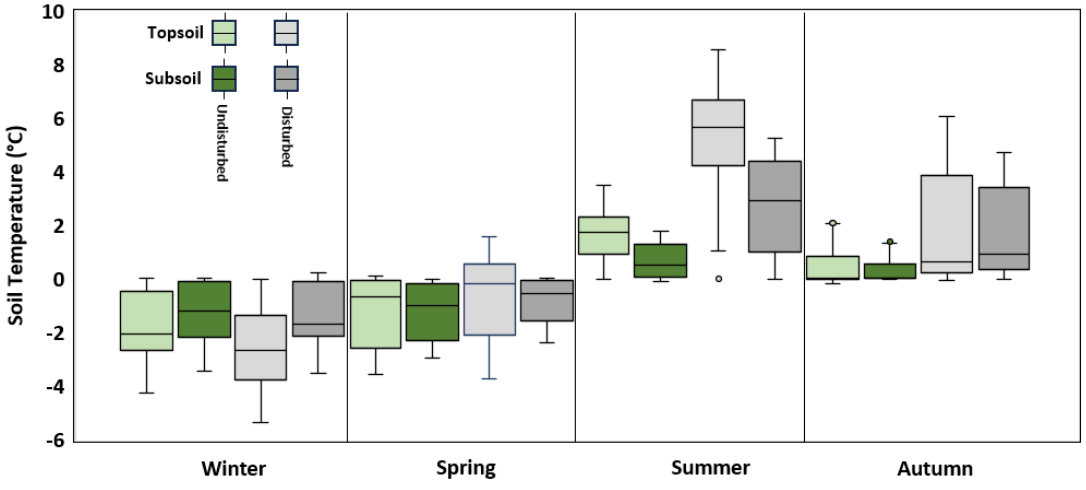

Figure 3. Seasonal soil temperature patterns. The seasons were delineated as winter (Nov–Mar), spring (Apr and May), summer (Jun–Aug), and autumn (Sep and Oct). Soil temperature are average daily values

from the topsoil and subsoil layers at the 8 chamber plots: 4 at the undisturbed site and 4 at the disturbed site. The range of the boxplot represents the first and third quartiles, while the central line signifies the median. The whiskers of the box extend to the minimum and maximum values, with outliers represented by circles.

VWC values ranged from 0.29+-0.00 m^3/m^3 to 0.47+-0.00 m^3/m^3 (1 Jun to 31 Oct 2024) (SI Figure S3). Subsoil layer exhibited elevated mean seasonal VWC values, as compared to the topsoil layer, at both locations (p values from 0.04 to < 0.001, ANOVA). Average maximum seasonal thaw depth exhibited significant differences between the two locations (p values 0.02, ANOVA), ranging from 58 ± 3 cm or 143 ± 29 cm at the undisturbed site or disturbed site, respectively (Figure 4). While the maximum seasonal thaw depth remained relatively consistent across the undisturbed plots, ranging from 50 cm to 61 cm, the disturbed plot displayed a larger range in maximum thaw depth, varying from 82 cm to 204 cm.

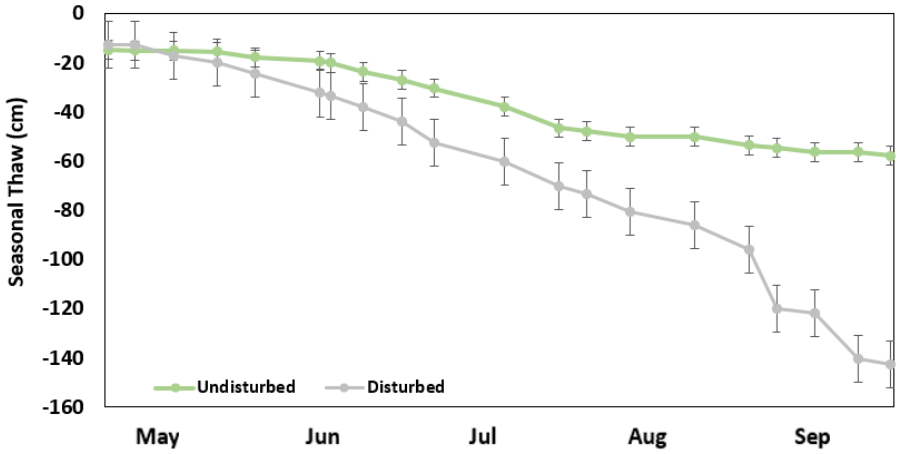

Figure 4. Average seasonal thaw depth at the undisturbed and disturbed sites measured using manual frost probe measurements from 12 May to 3 Oct 2023. Error bars are standard error.

3.2 Soil properties

The disturbance had a significant effect on LOI (a proxy for SOM content) in the subsoil layer, but not the topsoil layer (SI Figure S4). There was no significant effect of sampling date or significant interaction of sampling date and disturbance on LOI. Mean total C concentration for subsoil at the disturbed site was 2.7% (averaged across LiCor chamber plots and sampling dates), significantly greater than that of the undisturbed site mean of 1.7% (p < 0.01; ANOVA). Mean LOI for the topsoil layer was 0.122 and 0.142 for disturbed and undisturbed, respectively (not significantly different).

Similarly, the disturbance was a significant factor for soil total C concentration and total N concentration in the subsoil layer (p < 0.01 and p < 0.05, respectively; ANOVA), but not the topsoil layer (Figure 5), and there was no significant effect of sampling date or significant interaction of sampling date

and disturbance on either C or N. Mean total C concentration for the topsoil layer was 4.7% and 5.8% for disturbed and undisturbed, respectively (not significantly different). Mean total N concentration for subsoil at the disturbed site was 0.16%, significantly greater than that of the undisturbed mean of 0.13% ($p < 0.01$; ANOVA). Mean total N concentration for the topsoil was 0.19% and 0.25% for disturbed and undisturbed, respectively (not significantly different).

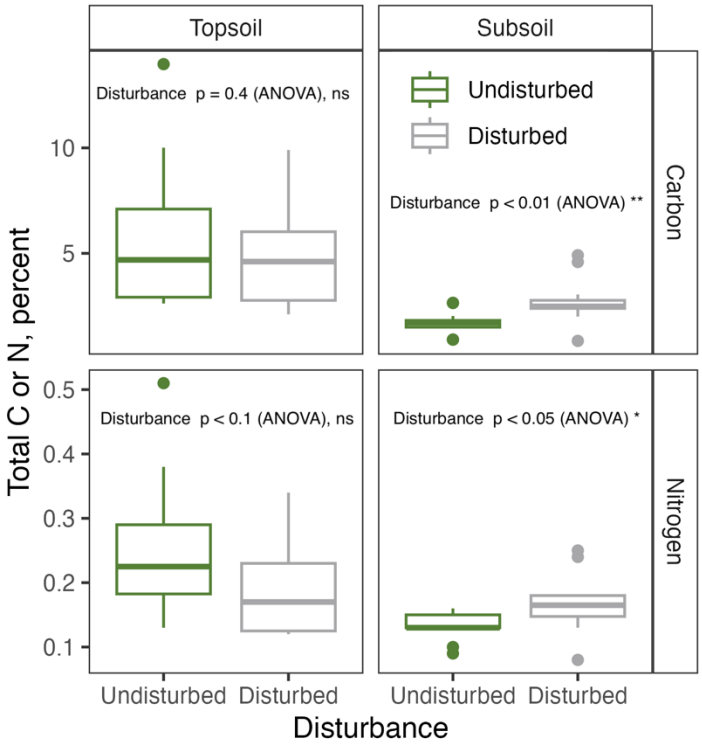

Figure 5. Soil total carbon and total nitrogen, at the disturbed and undisturbed sites. Boxplots represent all three sampling dates and four LiCor chamber plots, within each site.

Similar to the response of LOI, total C, and total N, soil pH was significantly different in the subsoil layer, depending on the site; the effect of disturbance on the topsoil layer was not significant (SI Figure S5). There was no significant effect of sampling date or significant interaction of sampling date and disturbance on soil pH. Mean pH for subsoil in the disturbed site was 4.63 (averaged across chambers and sampling dates), significantly greater than that of the undisturbed site mean of 4.11 ($p < 0.01$; ANOVA). Mean pH for the topsoil layer was 3.78 and 3.79 for disturbed and undisturbed, respectively (not significantly different).

3.3 Soil microbial community composition and diversity

We compared microbial community composition and diversity between the disturbed and undisturbed sites to enhance our understanding of the role that microbes play in soil respiration. By examining the effects of the site disturbance on microbial diversity—quantified through variations in species richness and community structure—we can ascertain which microbial groups exhibit the greatest sensitivity to environmental alterations and how their functional roles might adapt in response. The dominant bacterial phyla included *Proteobacteria*, *Acidobacteria*, *Actinobacteria*, *Verrucomicrobia*, and *Chloroflexi*, which together comprised over 75% of relative abundance (Figure 6). For fungi, 54% of relative abundance was comprised of *Ascomycota* (mostly classes *Leotiomycetes* and *Archaeorhizomycetes*), and 40% was *Basidiomycota* (mostly class *Agaricomycetes*) (Figure 6). Differential abundance testing only identified several dozen taxa (after filtering for somewhat higher abundance taxa) that were either significantly enriched or depleted under disturbance (see SI Figures S6 and S7). Notably, several Chloroflexi and Dormibacterota (a newly named phylum, previously identified as Chloroflexi) ASV's are depleted under disturbance relative to the undisturbed condition in subsoil, particularly at the February sampling date (SI Figure S7).

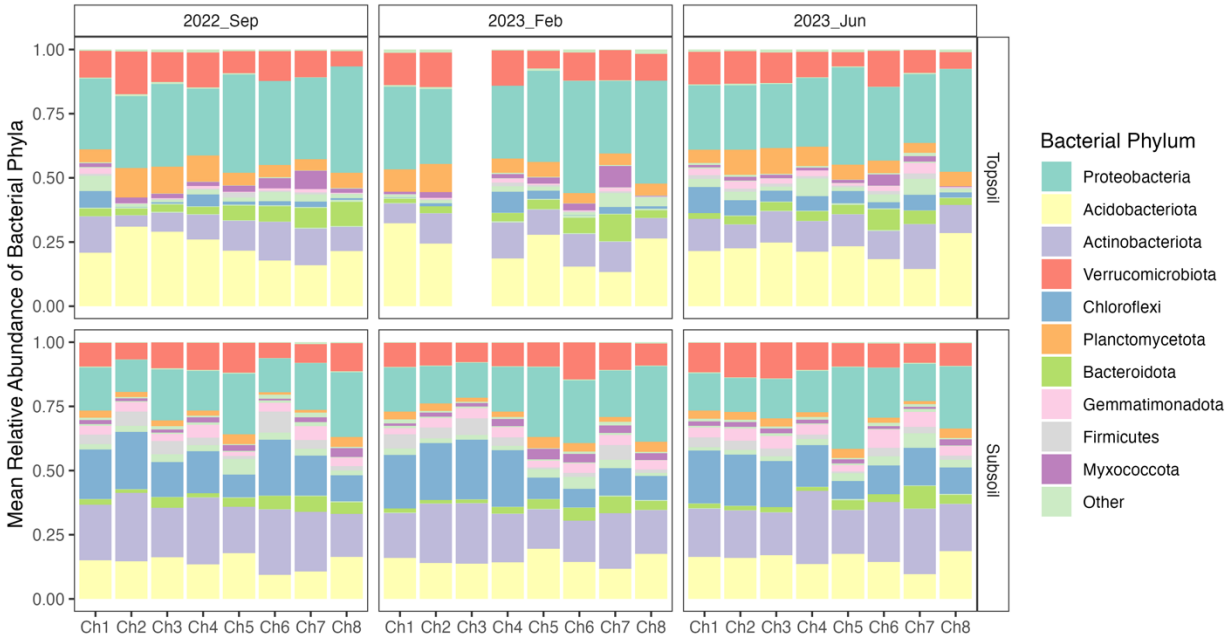

Figure 6. Relative abundances of dominant bacterial phyla, faceted by sampling date and soil layer. Each plot is named for LiCor chamber (Ch1 through Ch8); Ch1, Ch2, Ch3, Ch4 are undisturbed plots, and Ch5, Ch6, Ch7, Ch8 are disturbed plots. One sample was excluded from analysis (2023_Feb, Chamber 3, Topsoil).

385

386 **Figure 7**. Relative abundances of dominant fungal classes, faceted by sampling date and soil layer. Each
387 plot is named for LiCor chamber (Ch1 through Ch8); Ch1, Ch2, Ch3, Ch4 are undisturbed plots, and Ch5,
388 Ch6, Ch7, Ch8 are disturbed plots. One sample was excluded from analysis (2023_Feb, Chamber 3,
389 Topsoil).

390 Mean estimated bacterial richness across the dataset was 711.5 ASVs, with a significant
391 differences between the two sites (SI Figure S8). Overall, the disturbed samples had 30% higher richness
392 compared to the undisturbed samples ($p < 0.01$, ANOVA); within each date and soil layer combination,
393 only the February 2023 subsoil samples demonstrated a significant effect of disturbance ($p < 0.01$,
394 ANOVA). There was no effect of sampling date or soil layer, or interaction amongst the factors. Mean
395 estimated fungal richness across the dataset was 165 ASVs; there was no effect of disturbance, sampling
396 date, soil layer, or interaction amongst the factors (SI Figure S8).

397 Employing Bray-Curtis dissimilarities to assess beta diversity (Figure 8), we observed notable
398 differences between the undisturbed and disturbed sites, concerning both bacterial and fungal
399 communities in the topsoil and subsoil layers ($p < 0.001$ for all; $R^2 = 0.158, 0.178, 0.186, 0.115$ for
400 bacterial topsoil, bacterial subsoil, fungal topsoil, and fungal subsoil communities, respectively;
401 PERMANOVA). Sampling date did not have a significant effect.

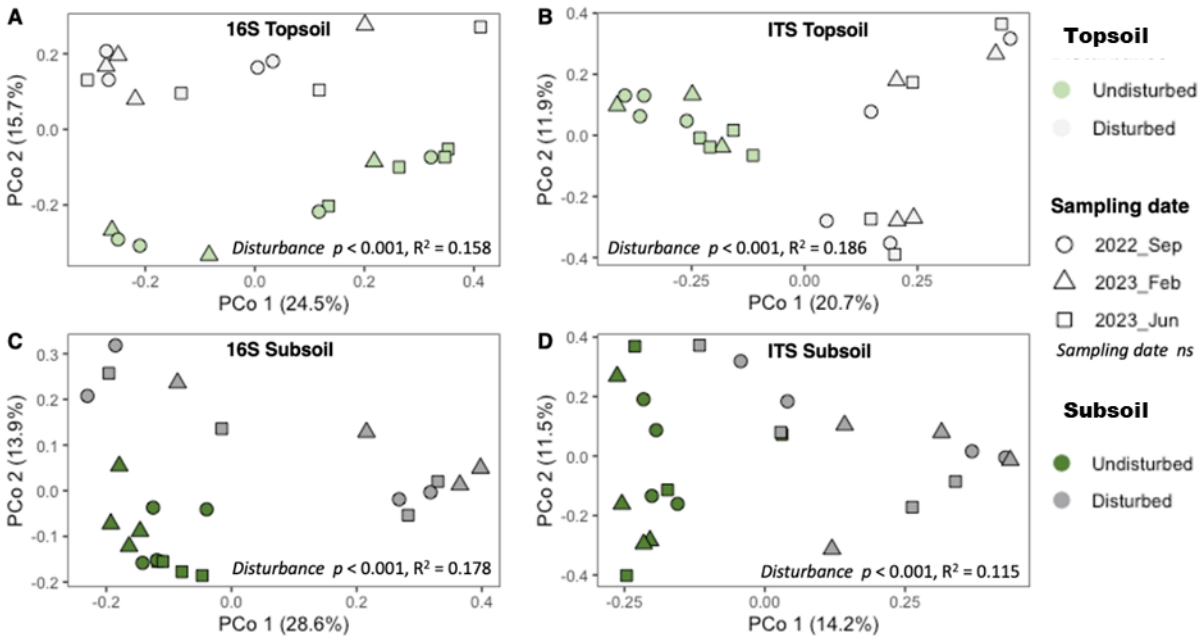

Figure 8. Principal coordinates analysis of Bray-Curtis dissimilarities of relative abundance data following rarefaction. Panels (A) and (C) represent the bacterial community (16S marker), and panels (B) and (D) represent the fungal community composition (ITS marker). The top panels (A & B; lighter shades) represent the topsoil layer community composition, while the bottom panels (C & D; darker shades) represent the subsoil community composition.

3.4 Soil Respiration

Total soil respiration rates showed distinct seasonal changes and were consistently higher, except during spring, at the disturbed site compared to the undisturbed one (Figure 9). The most significant activity occurred in the summer, with mean daily fluxes reaching 4.01 ± 0.12 g C-CO_2 m^{-2} d^{-1} at the undisturbed site and peaking at 4.81 ± 0.17 g C-CO_2 m^{-2} d^{-1} at the disturbed site, a statistically significant difference ($p < 0.0001$, ANOVA). Respiration rates declined in autumn, with mean daily fluxes of 1.79 ± 0.13 g C-CO_2 m^{-2} d^{-1} (undisturbed) and 1.91 ± 0.15 g C-CO_2 m^{-2} d^{-1} (disturbed). The mean daily fluxes decreased further in spring, measuring 1.46 ± 0.14 g C-CO_2 m^{-2} d^{-1} (undisturbed) and 1.41 ± 0.13 g C-CO_2 m^{-2} d^{-1} (disturbed); during these two shoulder seasons, the differences between the sites were not statistically significant. The lowest mean daily efflux was recorded during winter, with rates dropping to 0.33 ± 0.01 g C-CO_2 m^{-2} d^{-1} at the undisturbed site and 0.39 ± 0.13 g C-CO_2 m^{-2} d^{-1} at the disturbed site, which, similar to the summer mean daily efflux, was also a statistically significant difference ($p < 0.01$, ANOVA). Annually, the disturbed site had a higher average soil efflux (2.07 ± 0.11 g C-CO_2 m^{-2} d^{-1}) than the undisturbed site (1.81 ± 0.09 g C-CO_2 m^{-2} d^{-1}), with the highest single mean daily flux of 9.27 g C-CO_2 m^{-2} d^{-1} recorded on July 20 at the disturbed site.

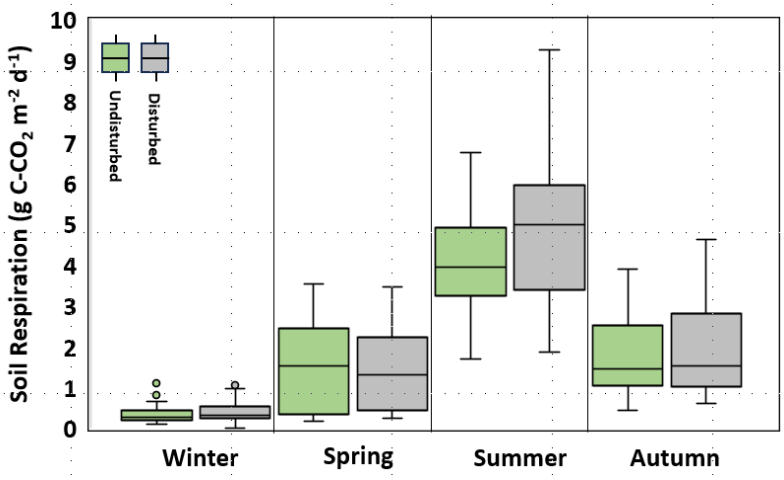

Figure 9. Seasonal soil respiration patterns observed at the undisturbed and disturbed sites. Soil respiration emissions are average diel fluxes from the 8 long-term chambers: 4 at undisturbed site and 4 at disturbed site. The range of the boxplot represents the first and third quartiles, while the central line signifies the median. The whiskers of the box extend to the minimum and maximum values, with outliers represented by circles.

3.5 Linear regression analysis to determine important variables contributing to soil efflux

A linear regression analysis was performed on the mean daily averages to investigate the seasonal correlation between soil efflux and various factors, including air temperature, barometric pressure, seasonal thaw depth, topsoil and subsoil temperature, and volumetric water content (VWC) at both undisturbed and disturbed sites. The analysis revealed that overall soil and air temperature exhibited the strongest correlation with soil respiration across all sites during different seasons. Soil and air temperatures showed the strongest correlations with soil efflux across all seasons. Seasonal R^2 values for soil temperatures ranged from 0.21–0.65 (winter), 0.87–0.92 (spring), 0.52–0.79 (summer), and 0.85–0.93 (autumn). Air temperature also correlated strongly with soil efflux in spring (R^2 = 0.74–0.77) and autumn (R^2 = 0.83–0.87). Moderate correlations were observed between soil efflux and thaw depth at both sites, with R^2 values ranging from 0.39–0.50 in spring, 0.41–0.43 in summer, and 0.74 in autumn.

The correlation between soil efflux and topsoil and subsoil VWC varied during the summer and fall seasons, as well as across the two soil layers. At the undisturbed site, in summer, moderate correlation was found in the topsoil (R^2 = 0.38) and strong in the subsoil (R^2 = 0.69). In autumn, correlations were strong in the topsoil (R^2 = 0.62) but weaker in the subsoil (R^2 = 0.22). At the disturbed site, in summer, the correlation was weak in the topsoil (R^2 = 0.09) but strong in the subsoil (R^2 = 0.64). In autumn, weak correlations were observed in both layers (R^2 = 0.28 in topsoil and 0.10 in subsoil). Regression analysis showed weak to no correlation between soil efflux and barometric pressure during winter and autumn (R^2

= 0.02–0.12) and no correlation in spring and summer. A slightly higher correlation was noted in winter when using hourly averages (R^2 = 0.23 undisturbed, 0.18 disturbed).

3.6 Random forest efflux modeling

The non-linear RF model effectively captured the impact of disturbance on the variation in soil respiration at both locations, showing strong confidence levels with high R^2 and moderate to low mean absolute error (MAE) values. Specifically, the model's R^2 values and corresponding MAE were 0.95 (0.14 MAE) for winter, 0.80 (0.38 MAE) for spring, 0.94 (0.16 MAE) for summer, and 0.82 (0.04 MAE) for autumn at the undisturbed site, and 0.95 (0.12 MAE) for winter, 0.83 (0.52 MAE) for spring, 0.96 (0.13 MAE) for summer, and 0.84 (0.05 MAE) for autumn at the disturbed site. Skewness and kurtosis values from the field data ranged from 0.04 - 1.24 and 1.61 - 4.56 at the disturbed site, and from 0.07 - 1.45 and 1.40 - 6.22 at the undisturbed site for all seasons, respectively. The ranges indicated that some instances contained a more normal distribution while other instances, especially winter, were notably skewed and tail-light and heavy.

The predictors' relative importance (RI) varied across seasons and sites (Figure 10). In the winter model at the undisturbed site, air temperature emerged as the most influential predictor, accounting for 53.6% RI. Conversely, at the disturbed site, the subsoil temperature exhibited the highest predictive power with 49.6% RI (figure 10). For the spring model, soil temperature was the best predictor at both sites, the topsoil layer temperature exhibited a slightly greater predictive power at the undisturbed site, whereas the subsoil layer temperature proved to be more influential at the disturbed site. In the undisturbed site's summer model, the soil moisture and temperature as well as the seasonal thaw depth variables exhibit similar RI values, ranging from 15.7 to 20.2%. Among these variables, air temperature has the lowest predictive power, with an RI of 10.3%. Conversely, at the disturbed site, the topsoil layer temperature stands out as the strongest predictor, with an RI of 44.6%. It is followed by the topsoil VWC, which has an RI of 13.7%. The undisturbed site's autumn model indicates that subsoil layer VWC has the highest predictive power at 24.3% RI, followed by subsoil layer temperature at 18.9% RI, and topsoil layer temperature at 18.7% RI. However, the disturbed autumn model shows that subsoil layer temperature is the most influential factor in predicting CO_2 efflux with 24.3% RI and topsoil layer (21.1% RI) and air (18.9% RI) also playing significant roles.

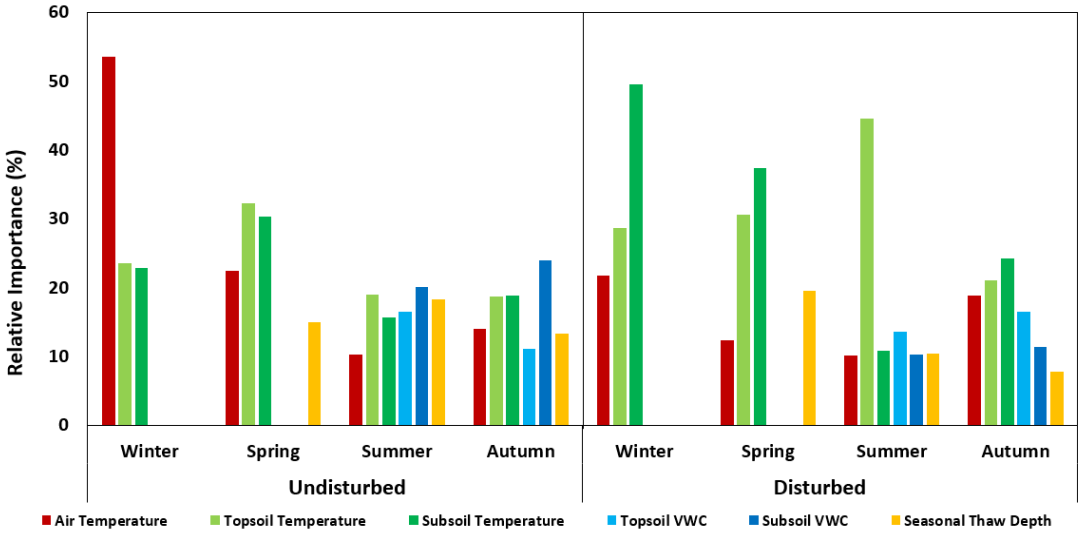

Figure 10. Relative importance (%) of variables to predict CO_2 efflux. Missing or static input variables (e.g. winter VWC and seasonal thaw depth) were not measured for importance.

Throughout the different seasons, various factors contribute to the varying degrees of relative importance regarding soil respiration. These factors include air temperature, the temperature of both topsoil and subsoil layers, and volumetric water content, which pertains only to subsoil. This information is presented in Table 1.

Table 1. Tabulation of the most important predictor variables to explain variability in the soil efflux data between disturbed and undisturbed sites as a function of season.

Season	Plot	Highest Predictor	RI
Winter	Undisturbed	Air temperature	53.6
Winter	Disturbed	Soil layer temperature (subsoil)	49.6
Spring	Undisturbed	Soil layer temperature (topsoil)	32.2
Spring	Disturbed	Soil layer temperature (subsoil)	37.4
Summer	Undisturbed	Volumetric water content (topsoil)	20.2
Summer	Disturbed	Soil layer temperature (topsoil)	44.6
Autumn	Undisturbed	Volumetric water content (subsoil)	24.0
Autumn	Disturbed	Soil layer temperature (subsoil)	24.3

4. Discussion

The primary objective of this study was to determine if an anthropogenic disturbance from approximately a century ago has a lasting legacy on carbon efflux in a boreal forest ecosystem. We

hypothesized that the disturbance would result in significant, persistent differences in soil respiration and edaphic properties between the disturbed and an adjacent undisturbed site. Crucially, we extended this hypothesis to the understudied winter period, postulating that these differences in soil activity would persist even under extreme cold temperatures. To elucidate the controls behind these variations, we examined seasonal CO_2 efflux alongside a suite of controlling factors, including soil temperature, moisture, soil organic matter, pH, seasonal thaw depth, and microbial community composition. In the following sections, we discuss how these interconnected variables explain the observed respiration patterns, providing insight into the long-term trajectory of carbon cycling following historical disturbance in permafrost environments.

Our findings show that the temperatures of the active layer soil were markedly elevated at the disturbed site in comparison to the undisturbed site (Figure 3). Previous research, conducted in similar subarctic environments, has attributed this increase in temperature, in disturbed environments, to a decrease in insulating organic matter (Gordon *et al*., 1987; Amiro, 2001; Yoshikawa et al., 2002; Koster et al., 2017 and 2018; Zhu et al., 2022) and alterations in surface albedo resulting from disturbance (Amiro, 2001; Yoshikawa et al., 2002; Koster et al., 2018; Zhu et al., 2022). The consequences of the modified thermal conditions were found to be significant, as the heightened soil temperatures affected biogeochemical cycles (Chatterjee *et al*., 2008; Akande et al., 2023) led to a deeper active layer (Forbes et al., 2002; Foster et al., 2022). In the current study, winter was the only season during which soil temperatures were elevated at the undisturbed site (Figure 3), as the unaltered surface vegetation provided a layer of insulation against the low air temperature. Snow did not influence the thermal conditions at the study locations, as both sites were devoid of snow during the winter to guarantee the proper functioning of the long-term chambers.

Disturbance had a significant impact on total carbon, total nitrogen (Figure 5), and soil pH in the subsoil layer (SI Figure S5). In the subsoil, the average total carbon concentration at the disturbed site was markedly higher than that at the undisturbed site (Figure 5). A comparable significant rise was noted for total nitrogen in the subsoil of the disturbed site when contrasted with the undisturbed site (Figure 5). Prior research has indicated that elevated carbon and nitrogen levels in the soil enhance soil respiration (Oertel et al., 2016, Akande et al., 2023, Schepaschenko et al., 2025). Nevertheless, in the topsoil layer, these effects were not statistically significant, implying that the increase in soil respiration was likely derived from the subsoil layer. Following this trend, soil pH in the subsoil was also significantly impacted, with the mean pH in the disturbed site being significantly higher than the mean at the undisturbed site.

Our results reveal a clear and persistent legacy of historical disturbance on soil carbon efflux, with the disturbed site exhibiting significantly higher overall respiration rates than the adjacent undisturbed site (Figure 9). This difference was most pronounced during the peak of the growing season, where summer CO_2 fluxes at the disturbed site were nearly 20% higher, a statistically significant margin ($p < 0.0001$). This finding strongly suggests that the initial disturbance—likely leading to warmer soils and a deeper active layer—has created conditions that continue to favor more rapid decomposition a century later. Interestingly, while respiration rates declined expectedly during the autumn and spring shoulder seasons, the differences between the two sites became statistically insignificant. This may indicate that during these transitional periods, other environmental factors, such as soil moisture levels or temperature thresholds, become more dominant controllers of microbial activity (Kim et al., 2012), temporarily masking the underlying differences in soil properties. Crucially, our data demonstrate that the elevated carbon loss at the disturbed site persists even into the winter. Although absolute fluxes were at their lowest, the wintertime respiration at the disturbed site was still significantly higher than at the undisturbed site ($p < 0.01$). This confirms that the ground remains a dynamic system and that the historical disturbance has altered the soil's thermal regime or substrate availability in a way that sustains higher microbial activity year-round, reinforcing the notion that winter is a critical (Natali et al., 2019; Miner et al., 2022), and often overlooked, period for carbon cycling in these ecosystems.

Beyond the direct physical and chemical changes, the historical disturbance also left a significant imprint on the soil's biological community. The effects of disturbance on microbial community structure were substantial, with significant alterations noted in both bacterial and fungal compositions (Figure 8). Notably, the date of sampling did not appear to influence community structure, indicating that the disturbance itself serves as the principal factor driving these changes. This finding is consistent with earlier studies that suggest soil disturbances can disrupt microbial habitats, resulting in a reorganization of community dynamics (Chatterjee *et al*., 2008; Dimitriu et al., 2010). Such changes can lead to cascading effects on ecosystem functions, including nutrient cycling and the decomposition of organic matter (Peng et al., 2008). We found that the disturbance-driven changes led to higher average soil temperatures and increased concentrations of mean SOM (LOI) (SI Figure S4), mean total carbon, and mean total nitrogen (Figure 5) in the subsoil, which positively influenced the mean annual soil respiration rates, resulting in an overall 14.4% increase when compared to the undisturbed site.

Our random forest model analysis found that key abiotic factors drive distinct seasonal patterns in soil efflux between the disturbed and undisturbed sites (Figure 10). In winter, air temperature emerged as the most significant predictor for the undisturbed sites, likely due to its direct impact on microbial activity and respiration rates. In contrast, the disturbed site during the same season showed a stronger correlation

with the subsoil layer temperature, suggesting that disturbances may alter the thermal dynamics of the soil profile, making soil temperature a more crucial determinant (Table 1). Moreover, given that both locations experienced snow denial, the more substantial ground vegetation cover at the undisturbed site offered superior thermal insulation to the soil, compared to the thinner ground cover vegetation at the disturbed site. Furthermore, it is very likely that winter soil respiration rates were higher at both sites where snow was not cleared, than at the chamber sites, as deep snow can provide an insulating effect as found by Welker et al. (2000) and Miner et al. (2022). During spring, topsoil layer temperature was the primary predictor for the undisturbed site, highlighting the importance of organic matter decomposition driven by temperature changes. For the disturbed site, the subsoil layer temperature remained the dominant factor, indicating that disturbances may have disrupted the organic layer, shifting the focus to the subsoil layer's thermal conditions.

In the summer months, the volumetric water content in the subsoil layer emerged as the principal predictor for the undisturbed site (Table 1), highlighting the essential role of moisture availability in influencing microbial activity and respiration during this warmer period. Conversely, the disturbed site exhibited a more pronounced correlation with the temperature of the topsoil layer (Table 1), indicating that disturbances may have modified the soil's hydrological characteristics by increasing thaw depth and enhancing drainage, which resulted in a reduced volumetric water content and rendered temperature a more significant factor than moisture. As autumn approached, the volumetric water content in the subsoil layer reestablished itself as the key predictor for the undisturbed site (Table 1), reaffirming the ongoing significance of moisture for microbial functions as temperatures began to decline. In contrast, for the disturbed site, the temperature of the subsoil layer continued to be the prevailing influence, underscoring the enduring effects of disturbances on the thermal dynamics of the soil. Other permafrost study sites in the arctic have shown a reliance of soil efflux on soil moisture and temperature and suggest the drying out of soil regimes and subsequent infiltration of snowmelt may also be a contributing factor for predicting soil efflux values (Welker et al., 2000) and therefore annual data collection may likely be necessary to determine long-term trends at sites where different soil types and disturbances exist. Overall, the observed patterns indicate that soil disturbances fundamentally alter the relationships between abiotic factors and CO_2 efflux. By reshaping thermal profiles and hydrological properties, disturbances intensify microbial activity across seasons, thereby increasing CO_2 emissions.

Conclusion

Permafrost-affected ecosystems are experiencing dramatic change from anthropogenic causes, both in terms of warming and physical disturbance to the soils. Active layers are deepening, unlocking

carbon that was previously inaccessible. Here, we sought to measure soil respiration in undisturbed and disturbed boreal forest sites to examine patterns of seasonality, the effect of legacy disturbance on soil system, and the influence of soil abiotic properties on respiration. This is particularly timely because our findings indicate that a historic disturbance in subarctic soils can have a lasting effect on the microbial community composition, but less so on the seasonal activity of the soils. The discovery of persistent microbial activity throughout the winter is critically significant, as future warming may prevent the active layer from fully refreezing, thereby intensifying year-round decomposition and carbon release. There were notable changes in soil temperature (162% warmer overall), the composition of bacterial communities (30% higher richness overall), total mean C (1% higher) and N (0.03% higher) concentration levels and pH (11.9% higher) values in the subsoil layer, and the depth of the maximum active thaw depth (147% deeper) as a result of disturbances, which subsequently led to 14.4% higher soil respiration rates. Soil respiration was primarily regulated by temperature, (air and soil) while factors such as soil volumetric water content and the depth of the active layer also contributed, with their relative importance varying throughout the different seasons. These findings underscore the complex interplay between seasonal variations, long lasting effect of soil and vegetation disturbance, and abiotic factors in determining soil respiration rates. Understanding these relationships is essential for accurate modeling of carbon cycling and for developing effective strategies to mitigate the impacts of soil disturbances on ecosystem functions. Both natural and anthropogenic disturbances can lead to a marked rise in the emission of carbon dioxide and other greenhouse gases into the atmosphere. Neglecting to account for these disturbances may result in a considerable underestimation of the role of soils in global carbon cycles. Future investigations should concentrate on the long-term consequences of these dynamics, especially considering ongoing warming change and its impact on permafrost regions.

Data availability. The datasets produced and/or examined in the present study can be obtained from the corresponding author upon reasonable request.

Author Contributions. DAV conceptualized the study and managed the data collection, RAB provided funding and insight on microbial data analysis, DAV, AJB, and WBB collected the soil samples, DAV and DB performed the soil respiration analysis, JRW performed the soil property and microbial community analyses. DAV drafted the initial manuscript and all authors contributed to revisions.

Competing Interests. The authors have no relevant financial or non-financial interests to disclose.

Acknowledgements. The authors express their gratitude to Ms. Elizabeth Corriveau for her work in conducting quality assurance and quality control on the soil respiration time series data and to Ms. Anne

Katula for her efforts in processing the soil samples for analyses related to microbial composition and soil properties.

Financial support. This work was founded by PE 0602144A Program Increase 'Defense Resiliency Platform Against Extreme Cold Weather'.

References

Akande, O.J., Ma, Z., Huang, C., He, F. and Chang, S.X., 2023. Meta-analysis shows forest soil CO2 effluxes are dependent on the disturbance regime and biome type. *Ecology Letters*, *26*(5), pp.765-777.

Amiro, B.D., 2001. Paired-tower measurements of carbon and energy fluxes following disturbance in the boreal forest. *Global Change Biology*, *7*(3), pp.253-268.

Anderson, M.J., 2001. A new method for non-parametric multivariate analysis of variance. *Austral ecology*, *26*(1), pp.32-46.

Apprill, A., McNally, S., Parsons, R. and Weber, L., 2015. Minor revision to V4 region SSU rRNA 806R gene primer greatly increases detection of SAR11 bacterioplankton. Aquatic Microbial Ecology, 75(2), pp.129-137.

Baker, C.C.M., Barker, A.J., Douglas, T.A., Doherty, S.J. and Barbato, R.A. 2023 Seasonal variation in near-surface seasonally thawed active layer and permafrost soil microbial communities *Environ Res Lett* **18** 055001

Barbato, R.A., Jones, R.M., Douglas, T.A., Doherty, S.J., Messan, K., Foley, K.L., Perkins, E.J., Thurston, A.K. and Garcia-Reyero, N., 2022. Not all permafrost microbiomes are created equal: Influence of permafrost thaw on the soil microbiome in a laboratory incubation study. *Soil Biology and Biochemistry*, *167*, p.108605.

Behnamian, A., Millard, K., Banks, S.N., White, L., Richardson, M. and Pasher, J., 2017. A systematic approach for variable selection with random forests: achieving stable variable importance values. IEEE Geoscience and Remote Sensing Letters, 14(11), pp.1988-1992.

Bonan, G.B., 2008. Forests and climate change: forcings, feedbacks, and the climate benefits of forests. *science*, *320*(5882), pp.1444-1449.

Bond-Lamberty, B., Bailey, V.L., Chen, M., Gough, C.M. and Vargas, R., 2018. Globally rising soil heterotrophic respiration over recent decades. *Nature*, *560*(7716), pp.80-83.

644 Bray, J.R. and Curtis, J.T., 1957. An ordination of the upland forest communities of southern
645 Wisconsin. *Ecological monographs*, *27*(4), pp.326-349.

646 Callahan, B.J., McMurdie, P.J., Rosen, M.J., Han, A.W., Johnson, A.J.A. and Dada, S.H., High-resolution
647 sample inference from Illumina amplicon data., 2016, 13. *DOI: https://doi.*
648 *org/10.1038/nmeth*, *3869*, pp.581-583.

649 Caporaso, J.G., Lauber, C.L., Walters, W.A., Berg-Lyons, D., Lozupone, C.A., Turnbaugh, P.J., Fierer, N.
650 and Knight, R., 2011. Global patterns of 16S rRNA diversity at a depth of millions of sequences
651 per sample. *Proceedings of the national academy of sciences*, *108*(supplement_1), pp.4516-4522.

652 Caporaso, J.G., Lauber, C.L., Walters, W.A., Berg-Lyons, D., Huntley, J., Fierer, N., Owens, S.M., Betley,
653 J., Fraser, L., Bauer, M. and Gormley, N., 2012. Ultra-high-throughput microbial community
654 analysis on the Illumina HiSeq and MiSeq platforms. *The ISME journal*, *6*(8), pp.1621-1624.

655 Chatterjee, A., Vance, G.F., Pendall, E. and Stahl, P.D., 2008. Timber harvesting alters soil carbon
656 mineralization and microbial community structure in coniferous forests. *Soil Biology and*
657 *Biochemistry*, *40*(7), pp.1901-1907.

658 Chi, J., Zhao, P., Klosterhalfen, A., Jocher, G., Kljun, N., Nilsson, M.B. and Peichl, M., 2021. Forest floor
659 fluxes drive differences in the carbon balance of contrasting boreal forest stands. *Agricultural and*
660 *Forest Meteorology*, *306*, p.108454.

661 Dimitriu, P.A. and Grayston, S.J., 2010. Relationship between soil properties and patterns of bacterial β-
662 diversity across reclaimed and natural boreal forest soils. Microbial ecology, 59(3), pp.563-573.

663 Doherty, S.J., Barbato, R.A., Grandy, A.S., Thomas, W.K., Monteux, S., Dorrepaal, E., Johansson, M. and
664 Ernakovich, J.G., 2020. The transition from stochastic to deterministic bacterial community
665 assembly during permafrost thaw succession. Frontiers in Microbiology, 11, p.596589.

666 Fekete, I., Kotroczó, Z., Varga, C., Nagy, P.T., Várbíró, G., Bowden, R.D., Tóth, J.A. and Lajtha, K.,
667 2014. Alterations in forest detritus inputs influence soil carbon concentration and soil respiration
668 in a Central-European deciduous forest. *Soil Biology and Biochemistry*, *74*, pp.106-114.

669 Forbes, B.C., Ebersole, J.J. and Strandberg, B., 2001. Anthropogenic disturbance and patch dynamics in
670 circumpolar arctic ecosystems. Conservation biology, 15(4), pp.954-969.

671 Foster, A.C., Wang, J.A., Frost, G.V., Davidson, S.J., Hoy, E., Turner, K.W., Sonnentag, O., Epstein, H., Berner,
672 L.T., Armstrong, A.H. and Kang, M., 2022. Disturbances in North American boreal forest and Arctic
673 tundra: impacts, interactions, and responses. *Environmental Research Letters*, *17*(11), p.113001.

Gordon, A.M., Schlentner, R.E. and Cleve, K.V., 1987. Seasonal patterns of soil respiration and CO2 evolution following harvesting in the white spruce forests of interior Alaska. *Canadian Journal of Forest Research*, *17*(4), pp.304-310.

Grace, J., 2004. Understanding and managing the global carbon cycle. *Journal of Ecology*, *92*(2), pp.189-202.

Harel, A., Sylvain, J.D., Drolet, G., Thiffault, E., Thiffault, N. and Tremblay, S., 2023. Fine scale assessment of seasonal, intra-seasonal and spatial dynamics of soil CO2 effluxes over a balsam fir-dominated perhumid boreal landscape. *Agricultural and Forest Meteorology*, *335*, p.109469.

Jorgenson, M.T., Douglas, T.A., Liljedahl, A.K., Roth, J.E., Cater, T.C., Davis, W.A., Frost, G.V., Miller, P.F. and Racine, C.H., 2020. The roles of climate extremes, ecological succession, and hydrology in repeated permafrost aggradation and degradation in fens on the Tanana Flats, Alaska. Journal of Geophysical Research: Biogeosciences, 125(12), p.e2020JG005824.

Kim, Y., Kimball, J.S., Zhang, K. and McDonald, K.C., 2012. Satellite detection of increasing Northern Hemisphere non-frozen seasons from 1979 to 2008: Implications for regional vegetation growth. Remote Sensing of Environment, 121, pp.472-487.

Kõljalg, U., Nilsson, R.H., Abarenkov, K., Tedersoo, L., Taylor, A.F., Bahram, M., Bates, S.T., Bruns, T.D., Bengtsson-Palme, J., Callaghan, T.M. and Douglas, B., 2013. Towards a unified paradigm for sequence-based identification of fungi.

Köster, E., Köster, K., Berninger, F., Aaltonen, H., Zhou, X. and Pumpanen, J., 2017. Carbon dioxide, methane and nitrous oxide fluxes from a fire chronosequence in subarctic boreal forests of Canada. *Science of the Total Environment*, *601*, pp.895-905.

Köster, E., Köster, K., Berninger, F., Prokushkin, A., Aaltonen, H., Zhou, X. and Pumpanen, J., 2018. Changes in fluxes of carbon dioxide and methane caused by fire in Siberian boreal forest with continuous permafrost. *Journal of environmental management*, *228*, pp.405-415.

Lei, Q., Yu, H. and Lin, Z., 2024. Understanding China's CO2 emission drivers: Insights from random forest analysis and remote sensing data. Heliyon, 10(7).

Martin, B.D., Witten, D. and Willis, A.D., 2021. Corncob: count regression for correlated observations with the beta-binomial.

Marty, C., Piquette, J., Morin, H., Bussières, D., Thiffault, N., Houle, D., Bradley, R.L., Simpson, M.J., Ouimet, R. and Paré, M.C., 2019. Nine years of in situ soil warming and topography impact the

temperature sensitivity and basal respiration rate of the forest floor in a Canadian boreal forest. *PLoS One*, *14*(12), p.e0226909.

Miner, K.R., Turetsky, M.R., Malina, E., Bartsch, A., Tamminen, J., McGuire, A.D., Fix, A., Sweeney, C., Elder, C.D. and Miller, C.E., 2022. Permafrost carbon emissions in a changing Arctic. Nature Reviews Earth & Environment, 3(1), pp.55-67.

Mölder, F., Jablonski, K.P., Letcher, B., Hall, M.B., Tomkins-Tinch, C.H., Sochat, V., Forster, J., Lee, S., Twardziok, S.O., Kanitz, A., Wilm, A., Holtgrewe, M., Rahmann, S., Nahnsen, S., and Köster, J. 2021). Sustainable data analysis with Snakemake. **F1000Research** 10:33. doi:10.12688/f1000research.29032.1

Natali, S.M., Watts, J.D., Rogers, B.M., Potter, S., Ludwig, S.M., Selbmann, A.K., Sullivan, P.F., Abbott, B.W., Arndt, K.A., Birch, L. and Björkman, M.P., 2019. Large loss of CO2 in winter observed across the northern permafrost region. Nature climate change, 9(11), pp.852-857.

Nilsson, R.H., Larsson, K.H., Taylor, A.F.S., Bengtsson-Palme, J., Jeppesen, T.S., Schigel, D., Kennedy, P., Picard, K., Glöckner, F.O., Tedersoo, L. and Saar, I., 2019. The UNITE database for molecular identification of fungi: handling dark taxa and parallel taxonomic classifications. *Nucleic acids research*, *47*(D1), pp.D259-D264.

Oertel, C., Matschullat, J., Zurba, K., Zimmermann, F. and Erasmi, S., 2016. Greenhouse gas emissions from soils—A review. Geochemistry, 76(3), pp.327-352.

Oksanen J, Simpson G, Blanchet F, Kindt R, Legendre P, Minchin P, O'Hara R, Solymos P, Stevens M, Szoecs E, Wagner H, Barbour M, Bedward M, Bolker B, Borcard D, Carvalho G, Chirico M, De Caceres M, Durand S, Evangelista H, FitzJohn R, Friendly M, Furneaux B, Hannigan G, Hill M, Lahti L, McGlinn D, Ouellette M, Ribeiro Cunha E, Smith T, Stier A, Ter Braak C, Weedon J (2024). _vegan: Community Ecology Package_. R package version 2.6-6.1, <https://CRAN.R-project.org/package=vegan>.

Pan, Y., Birdsey, R.A., Fang, J., Houghton, R., Kauppi, P.E., Kurz, W.A., Phillips, O.L., Shvidenko, A., Lewis, S.L., Canadell, J.G. and Ciais, P., 2011. A large and persistent carbon sink in the world's forests. *science*, *333*(6045), pp.988-993.

Parada, A.E., Needham, D.M. and Fuhrman, J.A., 2016. Every base matters: assessing small subunit rRNA primers for marine microbiomes with mock communities, time series and global field samples. *Environmental microbiology*, *18*(5), pp.1403-1414.

734 Parker, T.C., Clemmensen, K.E., Friggens, N.L., Hartley, I.P., Johnson, D., Lindahl, B.D., Olofsson, J.,
735 Siewert, M.B., Street, L.E., Subke, J.A. and Wookey, P.A., 2020. Rhizosphere allocation by
736 canopy-forming species dominates soil CO2 efflux in a subarctic landscape. *New*
737 *Phytologist*, *227*(6), pp.1818-1830.

738 Peng, Y., Thomas, S.C. and Tian, D., 2008. Forest management and soil respiration: Implications for carbon
739 sequestration. *Environmental Reviews*, *16*(NA), pp.93-111.

740 Quast, C., Pruesse, E., Yilmaz, P., Gerken, J., Schweer, T., Yarza, P., Peplies, J. and Glöckner, F.O., 2012.
741 The SILVA ribosomal RNA gene database project: improved data processing and web-based
742 tools. *Nucleic acids research*, *41*(D1), pp.D590-D596.

743 R-Core-Team, 2018. R: A Language and Environment for Statistical Computing, R Foundation for
744 Statistical Computing.

745 Rodtassana, C., Unawong, W., Yaemphum, S., Chanthorn, W., Chawchai, S., Nathalang, A., Brockelman,
746 W.Y. and Tor-ngern, P., 2021. Different responses of soil respiration to environmental factors
747 across forest stages in a Southeast Asian forest. *Ecology and Evolution*, *11*(21), pp.15430-15443.

748 Schepaschenko, D., Mukhortova, L. and Shvidenko, A., 2025. Estimation of Impact of Disturbances on Soil
749 Respiration in Forest Ecosystems of Russia. *Forests*, *16*(6), p.925.

750 Schonlau, M. and Zou, R.Y., 2020. The random forest algorithm for statistical learning. The Stata Journal,
751 20(1), pp.3-29.

752 Shiklomanov, N.I., Streletskiy, D.A., Little, J.D. and Nelson, F.E., 2013. Isotropic thaw subsidence in
753 undisturbed permafrost landscapes. Geophysical Research Letters, 40(24), pp.6356-6361.

754 Smith, D.P. and Peay, K.G., 2014. Sequence depth, not PCR replication, improves ecological inference
755 from next generation DNA sequencing. *PloS one*, *9*(2), p.e90234.

756 Soil Survey Staff. 2022. Keys to Soil Taxonomy, 13th edition. USDA Natural Resources Conservation
757 Service

758 Storer, D.A., 1984. A simple high sample volume ashing procedure for determination of soil organic
759 matter. *Communications in Soil Science and plant analysis*, *15*(7), pp.759-772.

760 Turetsky, M.R., Abbott, B.W., Jones, M.C., Anthony, K.W., Olefeldt, D., Schuur, E.A., Grosse, G., Kuhry,
761 P., Hugelius, G., Koven, C. and Lawrence, D.M., 2020. Carbon release through abrupt permafrost
762 thaw. *Nature Geoscience*, *13*(2), pp.138-143.

763 Vas, D.A., Corriveau, E.J., Gaimaro, L.W. and Barbato, R.A., 2023. Challenges and Limitations of Using
764 Autonomous Instrumentation for Measuring In Situ Soil Respiration in a Subarctic Boreal Forest
765 in Alaska, USA.

766 Walters, W., Hyde, E.R., Berg-Lyons, D., Ackermann, G., Humphrey, G., Parada, A., Gilbert, J.A.,
767 Jansson, J.K., Caporaso, J.G., Fuhrman, J.A. and Apprill, A., 2016. Improved bacterial 16S rRNA
768 gene (V4 and V4-5) and fungal internal transcribed spacer marker gene primers for microbial
769 community surveys. *Msystems*, *1*(1), pp.10-1128.

770 Watts, J.D., Natali, S.M., Minions, C., Risk, D., Arndt, K., Zona, D., Euskirchen, E.S., Rocha, A.V.,
771 Sonnentag, O., Helbig, M. and Kalhori, A., 2021. Soil respiration strongly offsets carbon uptake
772 in Alaska and Northwest Canada. *Environmental Research Letters*, *16*(8), p.084051.

773 Welker, J.M., Fahnestock, J.T. and Jones, M.H., 2000. Annual CO2 Flux in Dry and Moist Arctic Tundra:
774 Field Responses to Increases in Summer Temperatures and Winter Snow Depth. *Climatic*
775 *Change*. 44, 139-150.

776 West, J.R., Whitman, T., 2022. Disturbance by soil mixing decreases microbial richness and supports
777 homogenizing community assembly processes. *FEMS Microbiology Ecology,* 98, 1–11.

778 Wickham, H. and Wickham, H., 2016. *Data analysis* (pp. 189-201). Springer International Publishing.

779 Willis, A., Bunge, J. and Whitman, T., 2017. Improved detection of changes in species richness in high
780 diversity microbial communities. *Journal of the Royal Statistical Society Series C: Applied*
781 *Statistics*, *66*(5), pp.963-977.

782 Yilmaz, P., Parfrey, L.W., Yarza, P., Gerken, J., Pruesse, E., Quast, C., Schweer, T., Peplies, J., Ludwig, W.
783 and Glöckner, F.O., 2014. All-species Living Tree Project (LTP)" taxonomic frameworks. *Nucleic*
784 *Acids Res*, *42*, pp.D643-D648.

785 Yoshikawa, K., Bolton, W.R., Romanovsky, V.E., Fukuda, M. and Hinzman, L.D., 2002. Impacts of wildfire on the
786 permafrost in the boreal forests of Interior Alaska. *Journal of Geophysical Research:*
787 *Atmospheres*, *107*(D1), pp.FFR-4.

788 Zhu, X., Xu, X. and Jia, G., 2023. Recent massive expansion of wildfire and its impact on active layer
789 over pan-Arctic permafrost. Environmental Research Letters, 18(8), p.084010.